Plasma immersion ion implantation of the interior surface of a large cylindrical bore using an auxiliary electrode

X. C. Zeng, T. K. Kwok, A. G. Liu, P. K. Chu,[a] and B. Y. Tang
Department of Physics and Materials Sciences, City University of Hong Kong, 83 Tat Chee Avenue, Kowloon, Hong Kong

(Received 7 July 1997; accepted for publication 23 September 1997)

A model utilizing cold, unmagnetized, and collisionless fluid ions as well as Boltzmann electrons is used to comprehensively investigate the sheath expansion into a translationally invariant large bore in the presence of an auxiliary electrode during plasma immersion ion implantation (PIII) of a cylindrical bore sample. The governing equation of ion continuity, ion motion, and Poisson's equation are solved by using a numerical finite difference method for different cylindrical bore radii, auxiliary electrode radii, and voltage rise times. The ion density and ion impact energy at the cylindrical inner surface, as well as the ion energy distribution, maximum ion impact energy, and average ion impact energy for the various cases are obtained. Our results show a dramatic improvement in the impact energy when an auxiliary electrode is used and the recommended normalized auxiliary electrode radius is in the range of 0.1–0.3. © *1998 American Institute of Physics.* [S0021-8979(98)01001-9]

I. INTRODUCTION

Plasma immersion ion implantation (PIII) or plasma source ion implantation (PSII) is an innovative and fledgling technique to enhance the surface properties of materials such as metals, polymers, ceramics, and semiconductors.[1–4] It has a number of advantages over conventional beam-line ion implantation techniques. An appealing feature of PIII is that it is possible to implant surfaces that are not line-of-sight accessible. The interior surfaces of industrial components such as dies, bushings, pipes, and piston rings pose a formidable challenge to conventional ion implantation, and so inner surface modification using PIII has been a topic of practical interest in recent years.[5–15]

The sheath structure and its temporal evolution in a cylindrical bore without an auxiliary electrode has been investigated.[5–8] The ion-matrix sheath in a cylindrical bore of radius r_b has been calculated and the important length scale is the ion-matrix overlap radius, s_1, given by:[5]

$$s_1 = \sqrt{\frac{-4\epsilon_0\phi_t}{en_0}} \tag{1}$$

where ϕ_t is the negative sidewall bias and n_0 is the uniform ion density. Typical values of the ion-matrix overlap radius for $\phi_t = -100$ kV are $s_1 = 14.9$ cm when $n_0 = 10^9$ cm^{-3} and 4.7 cm when $n_0 = 10^{10}$ cm^{-3}. For zero rise-time voltage pulses and $r_b \leqslant s_1$, the bore is filled by an un-neutralized ion component. The ion charge in the bore is insufficient to completely shield the applied potential, and it can be categorized as a "small bore case." In a small bore ($r_b \leqslant s_1$), the potential drop from the axis to the sidewall in the ion-matrix sheath is given by:[5]

$$\Delta\phi = (r_b/s_1)^2\phi_t. \tag{2}$$

The temporal evolution of the potential, ion density, and ion velocity have been calculated in a small bore without a grounded auxiliary electrode positioned along the axis of a cylindrical bore specimen for a zero rise-time voltage pulse.[6] In this case, the sheath spans the bore at $t=0$ and then the ions in the bore decay with time. There is no sheath propagation and the maximum ion impact energy is only $0.3681|\Delta\phi|$, where $\Delta\phi$ is given by Eq. (2). The impact energy is lower for the more realistic finite rise-time voltage pulses.[7]

For zero rise-time voltage pulses and $r_b > s_1$, there is a region of neutral plasma around the axis and it is referred to as a "large bore case." The temporal dependence of the sheath width, sheath speed, and ion impact energy as well as the dependence of the maximum and average ion impact energy on the radius of the large bore without any auxiliary electrode have been investigated.[8] It is found that the sheath propagation speed increases as the radius decreases. After the sheath has reached the axis, the potential drop across the bore decays rapidly, and consequently, the ion impact energy first increases and then decreases in time. Both the maximum and average impact energy increase with the radius.

Previous studies have concluded that for PIII in a cylindrical bore, improving the impact energy is most crucial.[9–11] We propose the increase of the impact energy of ions implanted into the interior sidewalls of cylindrical specimens by using an auxiliary electrode which is a zero potential conductive cylindrical bar positioned along the axis of the implanted cylindrical bore. The structure of the ion-matrix sheath and its temporal evolution in a small cylindrical bore with an auxiliary electrode have been calculated for zero rise-time voltage pulses, and the impact energy increases significantly in the presence of an auxiliary electrode.[12,13] We have also computed the effects of the auxiliary electrode radius and the voltage pulses rise time for a small cylindrical bore with an auxiliary electrode.[14,15] It is found that the normalized auxiliary electrode radius should range from 0.10 to 0.30 in order to maximize the dose and produce a larger number of ions possessing high impact energy. The maximum ion impact energy and the average impact energy are

[a]Electronic mail: appkchu@cityu.edu.hk

 0021-8979/98/83(1)/44/6/$15.00

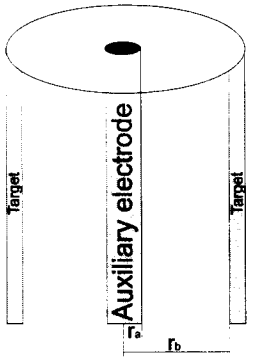

FIG. 1. Schematic of the problem considered. The plasma with a uniform ion density n_0 initially fills the space between a cylindrical bore and an auxiliary electrode. The radius of the bore is r_b and its potential is ϕ_t ($\phi_t<0$). The radius of the conductive auxiliary electrode is r_a and its potential is zero.

improved for finite rise-time voltage pulses and shorter rise times yield better results.

In this work, a comprehensive study on the time-dependent sheath in large bores ($r_b>s_1$) with an auxiliary electrode is conducted. We will describe the fluid modeling and formulation, and show the effects of the cylindrical bore radius, auxiliary electrode radius, as well as voltage pulse rise time on the ion impact energy.

II. FLUID MODELING AND FORMULATION

We consider PIII into the interior sidewall of a cylindrical bore with an auxiliary electrode as shown schematically in Fig. 1. The radius of the bore is r_b and the radius of the auxiliary electrode is r_a ($r_a<r_b$). The variable r measures the distance from the symmetry axis. The system is transitionally invariant along the axis of the bore, and it is azimuthally symmetrical, so that the variables only depend on r. When (r_b-r_a) is more than the Debye length, it is assumed that the bore is uniformly filled with a neutral plasma in which the density of electrons and ions are both n_0 and the potential is zero.[5] The electron is characterized by the electron temperature T_e. The ion mass is M and the ion charge is e. The initial ion velocity $v_i(0)$ is zero and the potential in the bore is given by:[16,17]

$$\phi_t=\begin{cases}\phi_p(t/t_r), & t\leqslant t_r\\ \phi_p, & t>t_r\end{cases}. \tag{3}$$

It is important to point out that the effects of the fall time of the voltage pulse is negligible as a pulse of sufficient duration will deplete almost all the ions within the bore and there are practically no ions left to experience the fall.[6]

This situation is modeled using cold, unmagnetized, and collisionless fluid ions, Boltzmann electrons, as well as the Poisson's equation.[7,18] In cylindrical coordinates, the equations of ion continuity and motion, Boltzmann's relationship, and Poisson's equation are:

$$\frac{\partial n_i}{\partial t}+\frac{1}{r}\frac{\partial}{\partial r}(rn_iv_i)=0, \tag{4}$$

$$\frac{\partial v_i}{\partial t}+v_i\frac{\partial v_i}{r}=-\frac{e}{M}\frac{\partial\phi}{\partial r}, \tag{5}$$

$$n_e=n_0\exp(e\phi/KT_e), \tag{6}$$

$$\frac{1}{r}\frac{\partial}{\partial r}r\frac{\partial\phi}{\partial r}=-\frac{e}{\epsilon_0}(n_i-n_e), \tag{7}$$

where $0<r_a\leqslant r\leqslant r_b$. The variables can be made dimensionless by normalization. The dimensionless variables used in this work are:

$$\rho=\frac{r}{S_1},\quad \Psi=\frac{\phi}{\phi_p},\quad N_i=\frac{n_i}{n_0},\quad V_i=\frac{v_i}{v_{\max}},\quad T=t\omega_{pi} \tag{8}$$

where $v_{\max}=\sqrt{-2e\phi_p/M}$ is the velocity the ion would have if it fell through a potential drop ϕ_p, and $\omega_{pi}=\sqrt{n_0e^2/\epsilon_0M}$ is the ion plasma frequency. In this way, the radius of the bore and the auxiliary electrode are $\rho_b=r_b/s_l$ and $\rho_a=r_a/s_l$, respectively. After substituting Eq. (6) into Eq. (7), the equations become:

$$\frac{\partial N_i}{\partial T}+\frac{1}{\sqrt{2}}\frac{1}{\rho}\frac{\partial}{\partial\rho}(\rho N_iV_i)=0, \tag{9}$$

$$\frac{\partial V_i}{\partial T}+\frac{1}{\sqrt{2}}V_i\frac{\partial V_i}{\partial\rho}=\frac{1}{2\sqrt{2}}\frac{\partial\Psi}{\partial\rho}, \tag{10}$$

$$\frac{1}{\rho}\frac{\partial}{\partial\rho}\rho\frac{\partial\Psi}{\partial\rho}=4[N_i-\exp(e\phi_p\Psi/KT_e)], \tag{11}$$

where $0<\rho_a\leqslant\rho\leqslant\rho_b$. Eq. (3) also becomes:

$$\Psi_t=\begin{cases}T/T_r, & T\leqslant T_r\\ 1, & T>T_r\end{cases}, \tag{12}$$

where $T_r=t_r\omega_{pi}$ is the dimensionless rise time.

Equations (9)–(11) are solved by finite difference methods. The discrete finite difference equations in the presence of an auxiliary electrode are:

$$N_{i,j+1}=N_{i,j}-\frac{f}{\sqrt{2}h(\rho_a+ih)}[hN_{i,j}V_{i,j}+(\rho_a+ih)\times(2N_{i,j}V_{i,j}-N_{i,j}V_{i-1,j}-N_{i-1,j}V_{i,j})] \tag{13}$$

$$V_{i,j+1}=V_{i,j}+\frac{f}{2\sqrt{2}h}[(\Psi_i-\Psi_{i-1})-2(V_{i,j})^2+2V_{i,}V_{i-1,j}] \tag{14}$$

$$\Psi_{i+1}(\rho_a+ih)+\Psi_i(h-2ih-2\rho_a)+\Psi_{i-1}(\rho_a+ih-h)=4h^2(\rho_a+ih)[N_{i,j}-\exp(-c\Psi_i)] \tag{15}$$

where $c=e|\phi_p|/KT_e$, h is the grid size in space, i.e., $\rho_{i+l}-\rho_i=h$, f is the time step used in our iteration, i.e., $T_{j+l}-T_j=f$, and i and j are positive integers. N_{ij}, V_{ij}, and Ψ_i are the normalized ion density, ion velocity, potential at normalized radii $\rho=\rho_a+ih$, and time $T=jf$, respectively. Note that the normalized potential ψ is not a direct function of T, and only N and V are partially differentiated with respect to T as shown in Eqs. (10) and (11). However, Ψ will indeed change with time as N will vary with T as indicated in Eqs.

(11) and (15). The boundary conditions are: $\Psi_0=0$ and $N_{0j}=0$ at $\rho=\rho_a$, and $\Psi_{(\rho_b-\rho_a)/h}=\Psi$, at $\rho=\rho_b$. The initial conditions are: $\Psi_i=0$, $V_{i,0}=0$, $N_{i,0}=1$ for $i>0$.

Equation (15) is solved via numerical iteration by first allowing ϕ to be an initial solution and linearizing Eq. (15) about this value using:[19]

$$\exp(-c\Psi)=\exp(-c\phi)\exp[-c(\Psi-\phi)]$$
$$=\exp(-c\phi)(1-c\Psi+c\phi). \quad (16)$$

After neglecting higher-order terms, Eq. (15) becomes

$$\Psi_{i+1}(\rho_a+ih)+\Psi_i[h-2ih-2\rho_a-4h^2(\rho_a+ih)c \times\exp(-c\phi)]+\Psi_{i-1}(\rho_a+ih-h)$$
$$=4h^2(\rho_a+ih)[N_{i,j}-\exp(-c\phi)-c\phi\exp(-c\phi)]. \quad (17)$$

We take ϕ from ψ of the previous time step, solve Eq. (17) to obtain a new ψ, set ϕ equal to this new ψ, and iterate until the process converges. Typically, it takes 2–3 iterations to converge.

The solved potential Ψ_i is then used to determine the normalized ion velocity V_{ij+1} and ion density N_{ij+1} of the next time step $j+1$ using Eqs. (13) and (14). The process of solving the potential at a time step as well as determining the ion velocity and ion density at the next time step is continued until the end of the simulation. A space grid $h=0.01$ and a time step $f=0.001$ are used in our simulation. When N is less than 0.001 at the target, the ions have been depleted. For $|\Phi_p|=50$ kV and $kT_e=5$ eV, c is equal to 10^4.

III. RESULTS AND DISCUSSION

Our numerical model is first checked by performing the simulation for $T_r=1$ and without the auxiliary electrode. Our results agree to within 0.2% of published results[8] thereby corroborating the validity of our model.

In order to study the effects of the bore radius, the cases for $\rho_a=0.3$, $T_r=5$, and $\rho_b=0.75$, 1.0, 1.5, 2.0, 2.5, and 3.0, are calculated. It is clear that the temporal dependence of the sheath width and the sheath speed is the same for the two cases with or without an auxiliary electrode before the sheath edge arrives at the auxiliary electrode.[8] When the sheath edge reaches the auxiliary electrode, the auxiliary electrode begins to improve the electric field in the sheath because its potential is kept at zero. The ions which still remain in the bore at this time will experience better acceleration. Without the auxiliary electrode, when the sheath arrives at the axis, the potential drop across the bore decays rapidly as the on-axis potential increases. As a consequence, the ion impact energy decays precipitously.[8] The temporal dependence of the dimensionless ion density N_{it} and ion impact energy E_{it} at the target for various ρ_b and $\rho_a=0.3$, $T_r=5$ are displayed in Fig. 2. The dimensionless ion impact energy is:

$$E_{it}=\frac{\frac{1}{2}Mv_{it}^2}{-e\phi_p}=\frac{\frac{1}{2}Mv_{it}^2}{\frac{1}{2}Mv_{max}^2}=V_{it}^2. \quad (18)$$

Here, v_{it} is the ion velocity at the target.

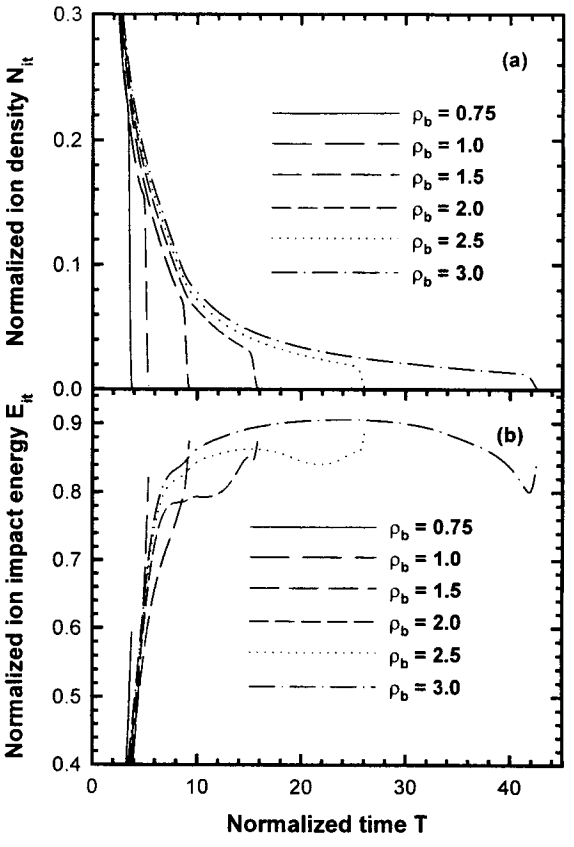

FIG. 2. Temporal dependence of (a) the dimensionless ion density N_{it} and (b) the dimensionless ion impact energy E_{it} [Eq. (18)] at the target for the bore radii $\rho_b=0.75$, 1.0, 1.5, 2, 2.5, and 3.0, when $\rho_a=0.3$ and $T_r=5$.

It is obvious that the time in which the ions in the bore are depleted increases rapidly with larger bore radius ρ_b. A larger ρ_b thus raises the ion impact energy and places a less stringent demand on the high-voltage pulse modulator. The rapid decrease in the ion impact energy reported at the tail without the auxiliary electrode[8] is not observed here, because the auxiliary electrode obviates the increase of the potential at the center of the bore. The ion impact energy shows undulation at the tail and around $T=7$. At around $T=7$, the bias is not continuous as it reaches the plateau value [Eq. (3)]. This phenomenon can also be observed in Figs. 5 and 7. The undulating at the tail region is due to two reasons. The impact energy is inversely proportional to the sheath speed[20] because the electric field in a rapidly expanding sheath decays more quickly than that in a slowly expanding sheath, and the sheath expanding speed is larger in the tail.[8] Therefore, the ion impact energy decreases mildly in the tail region. In addition, when the sheath reaches the auxiliary electrode, the electric field is improved. Its distribution in space is nonuniform and the electric field is larger near the auxiliary electrode.[13] Hence, undulating results as the remaining ions are accelerated and implanted into the target.

The time-integrated distributions of the ion-impact energies $f(E_{it})$ for $\rho_b=0.75$, 1.0, 1.5, 2, 2.5, and 3.0 and $\rho_a=0.3$, $T_r=5$ are depicted in Fig. 3. The distributions are normalized so that the integral over energy gives a unity ion dose. The number of high-energy ions increases with ρ_b. For

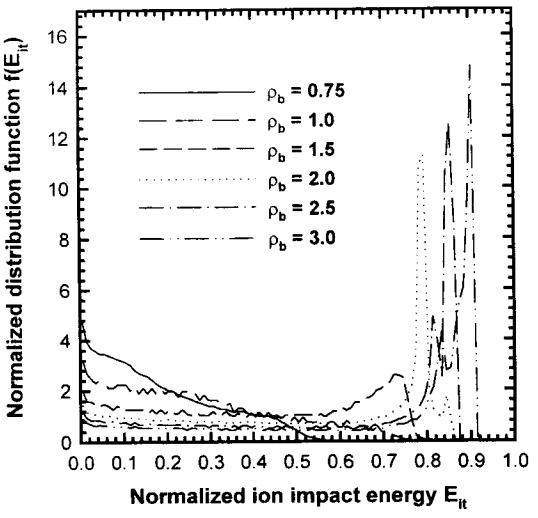

FIG. 3. Time-integrated distribution functions of ion impact energy $f(E_{it})$ for $\rho_b = 0.75$, 1.0, 1.5, 2.0, 2.5, and 3.0, when $\rho_a = 0.3$ and $T_r = 5$. The distributions are normalized so that the integral over energy gives the dimensionless ion dose equal to 1.

$\rho_b \leq 1$, there is no sharp high energy peak at the tail because the ions in the bore have already been exhausted before the potential at the target reaches the plateau value. When the radius of the impact bore ρ_b becomes large, more ions in the bore experience the slower sheath expansion and attain a higher ion impact energy, thereby producing the sharp high energy peak.

As shown in Fig. 4, the normalized maximum ion impact energy $E_{it\,\max}$ and the normalized average ion impact energy E_{itavg} both increase with the radius of the bore ρ_b. For $0.75 \leq \rho_b \leq 1.5$, the maximum impact energy increases rapidly with ρ_b as expected. However, the trend is milder when ρ_b is larger than 1.5 as the maximum impact energy now depends primarily on the sheath expansion. Since there are

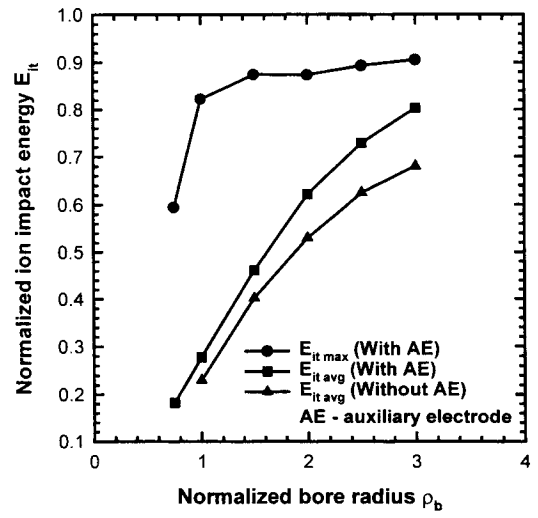

FIG. 4. Maximum normalized ion impact energy E_{itmax} and average normalized ion impact energy E_{itavg} vs normalized bore radius ρ_b for $\rho_a = 0.3$ and $T_r = 5$. The average dimensionless ion impact energy E_p for $T_r = 1$ and $\rho_a = 0$ (without any auxiliary electrode) is shown here for comparison.

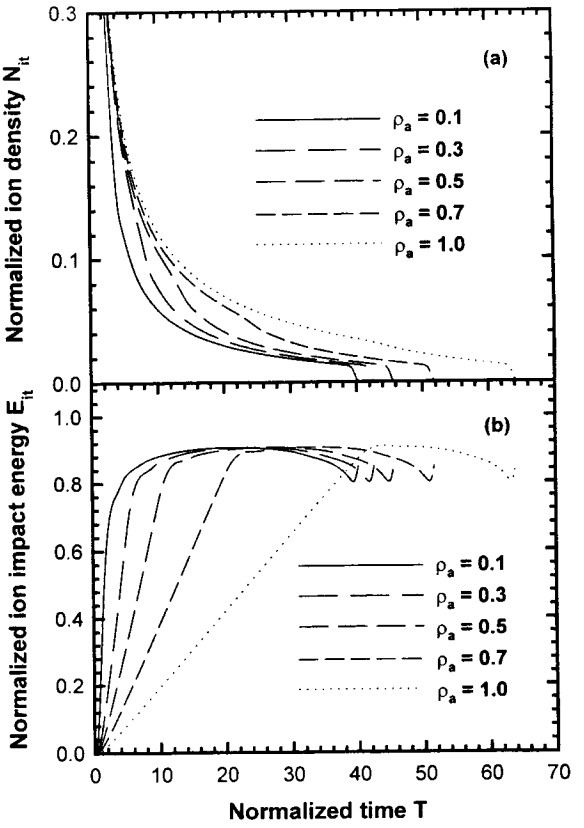

FIG. 5. Temporal dependence of (a) the dimensionless ion density of N_{it} and (b) the dimensionless ion impact energy E_{it} [Eq. (18)] at the target for auxiliary electrode radius $\rho_a = 0.1$, 0.3, 0.5, 0.7, and 1.0, when $\rho_b = 3.0$ and $T_r = 10$.

more ions experiencing the slower sheath expansion and thus possessing larger ion impact energy, the average ion impact energy increases with ρ_b. As previously mentioned, when the sheath reaches the auxiliary electrode, the electric field between the bore and the auxiliary electrode is improved and the remaining ions will get better acceleration. Therefore, the average ion impact energy is always larger when compared to the case without an auxiliary electrode (Fig. 4). In fact, the average ion impact energy is improved by at least 15% when an auxiliary electrode is employed. Figures 2–4 suggest that we should increase ρ_b in order to enhance the ion impact energy during PIII of the interior surface of a cylindrical bore. Practically, when ϕ_t and r_b are fixed (ϕ_t for a specific implantation depth and r_b dependent on the physical dimension of the target), we can increase the plasma density according to Eqs. (1) and (8).

The effects of the auxiliary electrode radius during PIII of a large bore for $\rho_b = 3.0$, $T_r = 10$, and $\rho_a = 0.1$, 0.3, 0.5, 0.7, and 1.0 are shown in Fig. 5 which depicts the temporal dependence of the dimensionless ion density N_{it} and impact energy E_{it} at the target versus the normalized time. The sheath expansion is the same before the sheath arrives at the auxiliary electrode. When the sheath reaches the auxiliary electrode, the electric field in the bore is affected. The rising and falling in the tail have been explained in the previous section. For $\rho_a = 1.0$, E_{it} only undulates mildly at the end because the sheath propagation speed is slow as the sheath

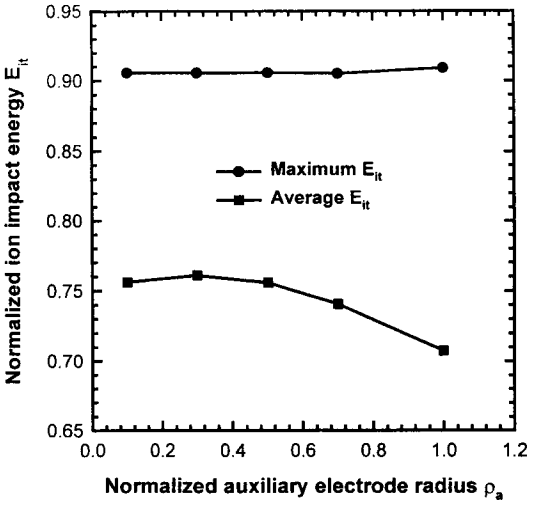

FIG. 6. Maximum normalized ion impact energy E_{itmax} and average normalized ion impact energy E_{itavg} vs normalized auxiliary electrode radius ρ_b for $\rho_a=0.3$ and $T_r=10$.

approaches the auxiliary electrode,[8] and the electric field between the bore and the auxiliary electrode is more uniform.[14] In contrast, for $\rho_a=0.1$, E_{it} shows a large rise and fall in the tail region [Fig. 5(b)] because the sheath propagation speed is fast when the sheath approaches the auxiliary electrode and the electric field between the bore and the auxiliary electrode is more nonuniform. Nonetheless, the maximum ion impact energy depends primarily on the sheath expansion in the bore for $\rho_b=3$, and the difference is quite small for $\rho_a=0.1$, 0.3, 0.5, 0.7, and 1.0 (Fig. 6). The number of high energy ions decreases with ρ_a ($\rho_a \geqslant 0.3$) as the sheath reaches the auxiliary electrode faster. The number of low energy ions is, however, the same for different ρ_a, and so the average ion impact energy E_{itavg} diminishes with ρ_a for $\rho_a \geqslant 0.3$ (Fig. 6). When $\rho_a=0.1$, the average ion impact energy shows only a small drop on account of the large rise and fall in the tail [Figs. 5(b) and (6)]. It can be concluded that ρ_a should range from 0.1 to 0.3 in order to achieve high ion impact energy. The results are consistent with our previous results derived for a small cylindrical bore.[14]

To investigate the effects of the voltage rise time, our model is solved for $\rho_b=3.0$, $\rho_a=0.3$, and $T_r=1$, 5, 10, 20, and 40. In a nitrogen plasma, these rise times correspond to $t_t=0.13$, 0.64, 1.27, 2.54, and 5.09 μs for $n_0=10^9$ cm^{-3}, and $t_r=0.04$, 0.20, 0.40, 0.80, and 1.61 μs for $n_0=10^{10}$ cm^{-3}. Figure 7 shows the temporal dependence of (a) the normalized ion density N_{it} and (b) the normalized ion impact energy E_{it} at the target. Since the sheath speed is similar when the sheath reaches the auxiliary electrode (ϕ_t has attained the plateau level) and the electric field between the bore and the auxiliary electrode is also similar (ρ_b and ρ_a are not variable), the ion impact energy shows a similar trend in the tail region. The number of low energy ions increases with T_r and the average ion impact energy E_{itavg} naturally decreases with the voltage rise-time T_r, as shown in Fig. 8. Consequently, the rule of thumb is to use a shorter rise-time voltage pulse when a high average ion impact energy is desired during PIII into the interior surface of a large cylindrical bore. Even though the potential at the target rises slowly for $T_r=40$, the bias has reached the plateau value before the sheath gets to the auxiliary electrode. The maximum ion impact energy thus depends mainly on the lowest sheath speed

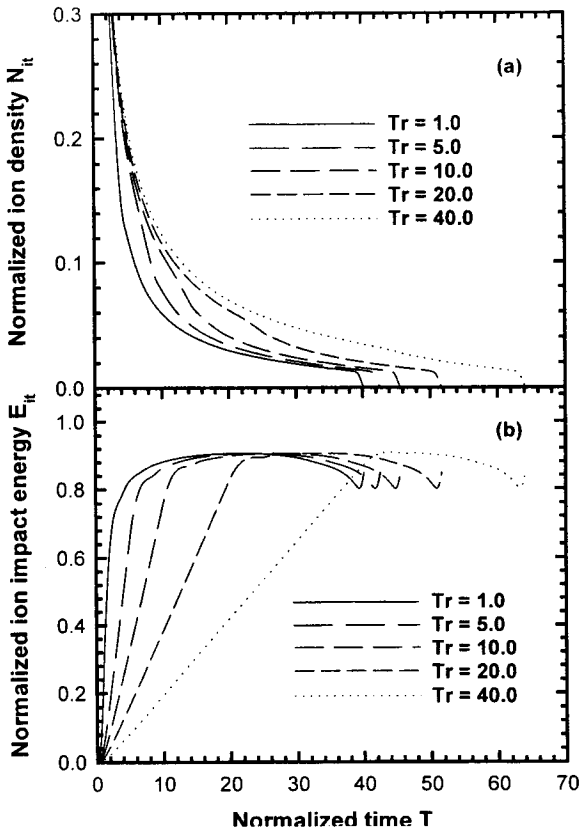

FIG. 7. Temporal dependence of (a) the dimensionless ion density N_{it} and (b) the dimensionless ion impact energy E_{it} [Eq. (18)] at the target for the dimensionless rise time $T_r=1$, 5, 10, 20, and 30, when $\rho_b=3.0$ and $\rho_a=0.3$.

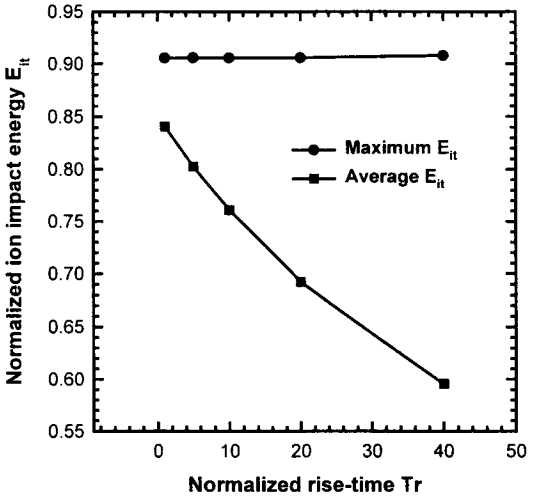

FIG. 8. Maximum normalized ion impact energy E_{itmax} and average normalized ion impact energy E_{itavg} vs normalized voltage rise time T_r for $\rho_b=3.0$ and $\rho_a=0.3$.

and is almost independent of the rise-time T_r as shown in Fig. 8.

IV. CONCLUSION

The sheath expansion into a large cylindrical bore with an auxiliary electrode has been investigated by solving the equations of ion continuity, ion motion, and Poisson's equation with a numerical finite difference method. The ion impact energy is improved significantly by using an auxiliary electrode. For example, the increase of the normalized average ion impact energy is more than 15% (Fig. 4). Moreover, the ion impact energy is higher if the bore radius ρ_b is larger. For instance, the normalized average impact energy for $\rho_a = 0.3$ and $T_r = 5$ increases from 28% when $\rho_b = 0.75\% - 80\%$ when $\rho_b = 3$. The main way to increase ρ_b is to use a higher plasma density. In addition, a fast high voltage modulator which can supply a shorter rise time and a large pulse current is necessary for PIII into a cylindrical bore because the average ion impact energy drops with increasing voltage rise time. Finally, given a fixed bore radius (specimen dependent) and rise time (hardware dependent), the suitable normalized auxiliary electrode radius is concluded to be in the range of 0.1–0.3 for both a small or large cylindrical bore if high ion impact energy is desired.

ACKNOWLEDGMENTS

The work is supported by Hong Kong Research Grants Council Central Allocation Grants 8730005, Hong Kong Research Grants Council Earmark Grant 9040220, and City University of Hong Kong Strategic Grant 7000730.

[1] J. R. Conrad, J. L. Radtke, R. A. Dodol, F. J. Worzala, and N. C. Tran, J. Appl. Phys. **62**, 4591 (1987).
[2] G. A. Collins, R. Hutchings, J. Tendys, and M. Samandi, Surf. Coat. Technol. **68/69**, 285 (1994).
[3] P. K. Chu, S. Qin, C. Chan, N. W. Cheung, and L. A. Larson, Mater. Sci. Eng. Rep. **R17**, 207 (1996).
[4] J. V. Mantese, I. G. Brown, N. W. Cheung, and G. A. Collins, MRS Bull. **21**, 52 (1996).
[5] T. E. Sheridan, J. Appl. Phys. **74**, 4903 (1993).
[6] T. E. Sheridan, Phys. Plasmas **1**, 3485 (1994).
[7] T. E. Sheridan, Surf. Coat. Technol. **85**, 204 (1996).
[8] T. E. Sheridan, J. Appl. Phys. **80**, 66 (1996).
[9] T. E. Sheridan, Phys. Plasmas **3**, 3507 (1996).
[10] M. Sun, S. Yang, and B. Li, J. Vac. Sci. Technol. A **14**, 367 (1996).
[11] M. Sun and S. Yang, J. Vac. Sci. Technol. A **14**, 3071 (1996).
[12] X. Zeng, B. Tang, and P. K. Chu, Appl. Phys. Lett. **69**, 3815 (1996).
[13] X. C. Zeng, T. K. Kwok, A. G. Liu, P. K. Chu, B. Y. Tang, and T. E. Sheridan, Appl. Phys. Lett. **71**, 1035 (1997).
[14] X. C. Zeng, T. K. Kwok, A. G. Liu, P. K. Chu, and B. Y. Tang, 24th IEEE International Conference on Plasma Science and Technology, San Diego, CA, May 19–22, 1997.
[15] X. C. Zeng, T. K. Kwok, A. G. Liu, P. K. Chu, and B. Y. Tang, 24th IEEE International Conference on Plasma Science and Technology, San Diego, CA, May 19–22, 1997.
[16] I. T. Scheuer, M. Shamin, and J. R. Conrad, J. Appl. Phys. **67**, 1241 (1990).
[17] R. A. Stewart and M. A. Lieberman, J. Appl. Phys. **70**, 3481 (1991).
[18] M. Widner, I. Alexeff, W. D. Jones, and K. E. Lonngren, Phys. Fluids **13**, 2532 (1970).
[19] G. A. Emmert and M. A. Henry, J. Appl. Phys. **71**, 113 (1992).
[20] T. E. Sheridan and M. J. Goeckner, J. Appl. Phys. **77**, 4967 (1995).